UDC 532.5, 537.39 PACS: 68.03.Hj
EDN: UOKBNM

Visualization of the electric field in transformer oil using suspended water microdroplets

© V. A. Panov*, A. S. Saveliev, Yu. M. Kulikov

*Joint Institute for High Temperatures of the Russian Academy of Sciences,
Moscow, 125412 Russia*
** E-mail: panovvladislav@gmail.com*

Received 10.03.2025; revised 02.04.2025; accepted 07.04.2025
Scientific specialty code 1.3.9

A method for visualizing electric field lines in a dielectric based on electrohydrodynamic (EHD) destruction of small droplets is proposed. The advantage of the method is a significantly lower seeding density of tracers as compared to solid particles, which reduces the influence of the dispersed phase on the resulting EHD flow and electrical strength of the medium. The proposed approach allows introducing destructible tracer drops into individual areas under study, including into the area of lower potential values, which reduces the probability of partial breakdowns during diagnostics. The effectiveness of the approach is confirmed by comparing experimental visualization data with calculation results.

Keywords: electric field lines; visualization; high-voltage oil-filled equipment; EHD streaming; Taylor cone; droplets; water.

DOI: 10.51368/1996-0948-2025-2-62-68

Introduction

The behavior of drops in an electric field has been attracting the interest of scientists for many decades. The results of these studies have found application in various fields such as meteorology [1, 2] (raindrops), liquid drop model in nuclear fission [3], (movement) of aerosols [4]. A hundred years ago, Zeleny [5], as well as Wilson and Taylor [6], proved by way of the experiment that a drop suspended in a capillary (pendant drop) and a soap bubble attached to a plate (sessile soap bubble) experience deformation in the electric field. What is more important, however, when electric field strength modulus on the surface of the pendant drop and sessile bubble was high enough, they became conical and emitted a thin stream that broke up into droplets. Papers [7, 8] discovered the similar behaviour exhibited in the presence of the electric field by a spherical pendant drop, which was initially electrically neutral. Unlike the pendant drop and sessile soap bubble, a neutral drop in the strong electric field forms two opposite conical ends and emits streams of positively and negatively charged droplets in opposite directions. The conical menisci formed in the electric field are now known as Taylor cones [9], while emission of thin streams from cone tips is referred to as electrohydrodynamic (EHD) tip streaming [10] or cone EHD streaming [11].

The findings of many authors allow to reveal the universality of these phenomena: emission of charged streams from conical surfaces and their decomposition into aerosols consisting of charged micro (nano) droplets (electrospraying) are common to various, allegedly unrelated situations during production processes and natural phenomena, including electrospray ionization mass spectrometry (ESIMS) [12], raindrops in thunderclouds [13], as well as printing and coating [14].

The droplet electrohydrodynamics has advanced into an independent discipline due to the papers of Taylor [15, 16], who gave criticism of previous research in this area and proposed his own theoretical leaky dieletric model (LDM). He also described stable minor deformation of a (single-phase) droplet. Later this model was repeatedly tested, and more accurate models emerged [15–21]. The subsequent works researched the complex topologies of interphase boundaries associated with multiphase emulsion droplets, the development of instabilities in emulsions, their decomposition (demulsification), and control of microparticles movement at the interphase boundary.

Although this area has been researched for many decades, most research efforts are of an academic nature, and only recently a series of works of applied significance has appeared [22–34].

The present study aims to extend the findings of droplet electrohydrodynamics to high-voltage engineering problems. This paper proposes the method for visualizing electric field lines, which is based on the comparison of laboratory and numerical experiments findings. The approach is based on visualizing trajectories of microdroplets formed as a result of decomposition of streams flowing from conical menisci of drops (Taylor cones) under the influence of the electric field.

Experimental setup

The experimental setup diagram is shown in the figure. 1. Two immiscible liquids are poured into vessel (1) with plane-parallel transparent walls made of organic glass: poorly conducting water (2) and transformer oil (3). A pointed high-voltage needle electrode (4) and a cylindrical electrode (5) with a rounded edge at the working end, which is connected to the "ground" through measuring resistor R_s with a resistance of 25 Ω, are immersed in oil and water, respectively. The voltage is supplied through the limiting resistor R_b (5 kΩ) to electrode (4) using semiconductor high-voltage switch (6) of the "half-bridge" type when a rectangular TTL pulse is formed at its input using digital pulse generator G. The voltage rise and fall front at the output of switch (6) is about 0.1 μs, which is much faster than the phenomena described herein.

The voltage amplitude was $V_0 = 20$ kV, and the open state duration of switch (6) was 400 μs. Since the high-voltage source ("DC" Fig. 1) cannot provide the sufficient output current (hundreds of milliamps) in case of breakdown of the interelectrode gap, high-voltage storage capacitor C with the capacity of 0.7 μF is added to the electrical circuit in parallel with the source. To measure the voltage on high-voltage electrode (4), a high-voltage probe 1:1000 is connected at point A, and a signal from this probe is sent to the digital storage oscilloscope.

To measure the current in the circuit, the voltage at point B is supplied to the oscilloscope. A signal from generator G, as well as an exposure sync pulse from high-speed digital video camera (8), are sent to other channels of the oscilloscope.

To visualize the occurring processes, background lighting (incandescent lamp (7)) and video camera (8) are used, with container (1) placed in between. The video camera lens is focused on the plane containing the electrode axis. The electrical breakdown is forced in liquids in advance according to the mechanism described in [35–37]. As a result, small (about 50 μm) water droplets appear in the oil in the interelectrode region (9). Since the lens depth of field is relatively small, the droplets that are close to the straight line containing the electrode axes can be seen as dark circles (Fig. 2). The droplets that are farther from this line, i.e. beyond the lens depth of field can be seen as fuzzy rings or half rings (Fig. 3). After water droplets are formed in the interelectrode space, the potential difference develops between the electrodes to deform and destroy them (Fig. 3).

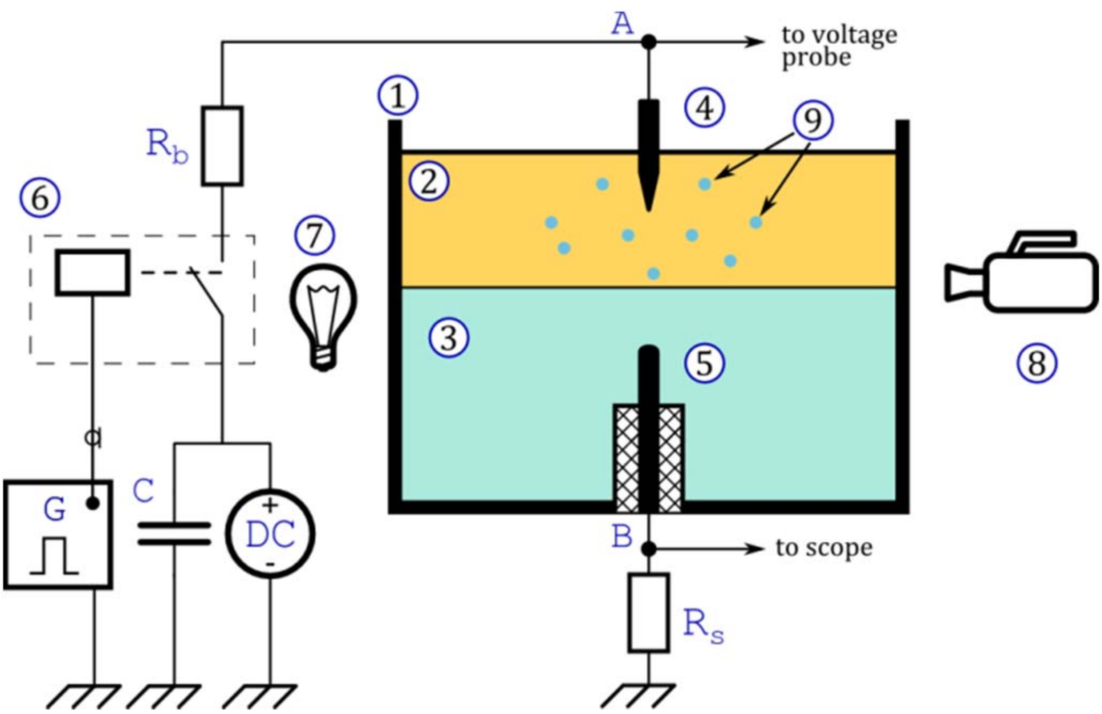

Fig. 1. Experimental setup diagram

Mathematical model

The problem is modeled in the axisymmetric setup. The electrode system is assumed to be immersed in a cylinder of 80 mm in diameter which is equal to the side of the experimental cell. The tip of the oil-immersed electrode is 3 mm away from the interphase boundary, the total thickness of the oil layer is 15 mm, the distance from the pin electrode surface to the interphase boundary is also 3 mm. The diameter of the cylindrical section of the pointed electrode is 1 mm, that of the cylindrical electrode – 1.8 mm. The radius of the needle tip rounding is 70 μm. Properties of materials filling the subdomains of calculation: water with relative permittivity $\varepsilon_w = 78$, transformer oil with $\varepsilon_o = 2$. Since liquids are considered to be ideal dielectrics, the electrostatic approximation described by the below system of equations is used:

$$\vec{E} = -\nabla V,$$
$$\vec{D} = \varepsilon \vec{E},$$
$$\nabla \cdot \vec{D} = \rho_v,$$

where $\vec{E}$ – electric field vector, V – electrostatic potential, $\vec{D}$ – electric displacement vector, ε – relative permittivity of the medium, ρ_v – volume charge density.

Spatial discretization of the system of equations is based on the finite element method. Values in cells are interpolated using second-order Lagrange polynomials. The following conditions are set at the boundaries: 1) condition of axial symmetry, 2) high-voltage potential V_0 = 20 kV is set on the surface of the pointed electrode, 3) zero charge ($\vec{n} \cdot \vec{D} = 0$), 4) zero potential (grounding) is set on the surface of the cylindrical electrode. The domain of calculation is covered with a triangular mesh of the finer size near the high-voltage electrode to ensure the best resolution of high voltage values. The maximum size of an element within the medium volume is 1 mm, the minimum size is 10 μm. The element size at the boundary of the high-voltage electrode does not exceed 10 μm. The total amount of mesh elements is 505,516 cells. The relative tolerance of the iterative solver is 0.001. Due to the small size of droplets as compared to the size of the discharge gap, the electric field is calculated without considering their presence.

Results and discussion

The figure 2 shows the image of the discharge gap and visible part of electrodes before the voltage pulse is applied. Water droplets acting as future tracers of electric field lines look like dark circles in the upper half of the image occupied by transformer oil. The dark strip adjacent to the water-oil interface is a shadow of the water meniscus that appears on the wall of the discharge cell at the stage of droplet formation through the electrical breakdown of the same gap. The misalignment of electrodes which can be seen on the photo is caused only by the difference in refractive indices of water and oil and the camera' set angle of view. Prior to the experiment the alignment is checked by directly touching the two electrodes on their axis.

Figure 3 shows water droplets before and at the end of voltage pulse sending. Initially, spherical droplets (top figure, 0 μs) begin to deform under the impact of the external electric field: they are stretched along the electric field lines. The visualization of electric field lines becomes even more adequate for the droplets, at which poles pointed peaks emitting fine droplets are formed. For example, droplet 1 in figure 3, by the end of the pulse, has almost completely decomposed into two clouds of fine droplets towards the high-voltage and grounded electrodes due to being in the region of the stronger field as compared to droplets 2 and 3. Droplet 2 is also fragmented, but since it is far from the electrode, the droplet is more drawn out and less streamed, which has beneficial for the quality of visualization of the electric field lines. The comparison with the calculated pattern of the electric field lines shown in the lower part of figure 3 reveals that the course of the lines is well aligned with the direction of deformation and streaming of the droplets.

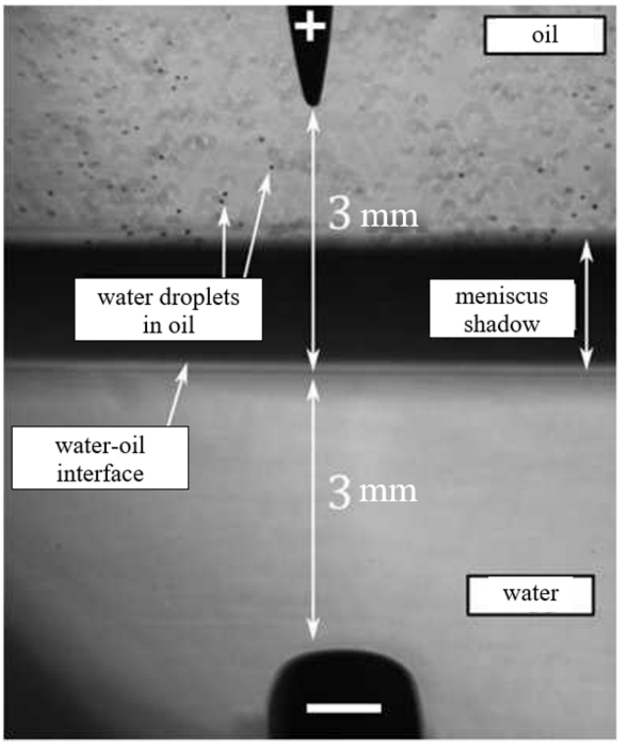

Fig. 2. View of the discharge gap before the voltage pulse is sent

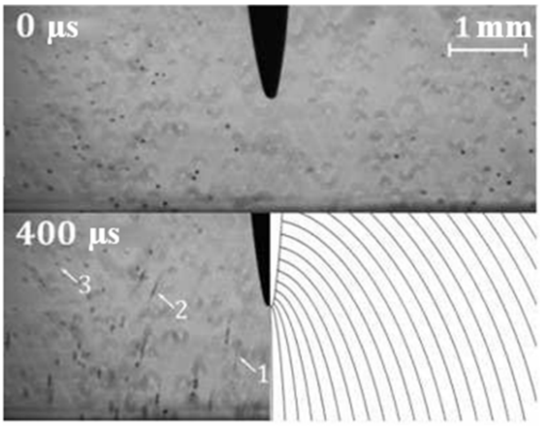

Fig. 3. Deformation and streaming of water droplets distributed in oil under the action of the voltage pulse with the amplitude of 20 kV and a duration of 400 µs (moments 0 and 400 µs). The second half of the lower image is supplemented with the calculated pattern of the electric field lines which was built for the experimental parameters

Conclusions

The method for visualizing the pulsed electric field lines in a dielectric liquid, which consists in observing the direction of deformation and streaming of droplets of a second liquid placed in the first one, has been proposed. The method has been tested using the water droplets placed in transformer oil, with the pulsed voltage fed to the needle-shaped high-voltage electrode. With the droplets used as tracers, the response time of the droplets to the external field and their noticeable deformation is only 100 µs in the experiment conditions under consideration. The fragmentability of droplets lowers the requirements for the tracer seeding density and also allows positioning them locally in the area of concern. With the lower seeding density, the impact on the electrical strength of the medium is decreased, which reduces the probability of partial breakdowns during diagnostics.

REFERENCES

1. Rayleigh L., Philos Mag **14** (87), 184–186 (1882).

2. Sartor J. D., Physics Today **22** (8), 45–51 (1969).

3. Bohr N. and Wheeler J. A., Physical Review **56** (5), 426–450 (1939).

4. Taflin D. C., Ward T. L. and Davis E. J., Langmuir **5** (2), 376–384 (1989).

5. Zeleny J., Physical Review **10** (1), 1–6 (1917).

6. Wilson C. T. R. and Taylor G. I., Mathematical Proceedings of the Cambridge Philosophical Society **22** (5), 728–730 (1925).

7. Nolan J., Proc R Ir Acad Sect A **37**, 28–39 (1926).

8. Macky W., Proceedings of the Royal Society of London. Series A. Containing Papers of a Mathematical and Physical Character **133** (822), 565–587 (1931).

9. Taylor G., Proceedings of the Royal Society of London. Series A. Mathematical and Physical Sciences **280** (1382), 383–397 (1964).

10. Collins R. T., Jones J. J., Harris M. T. and Basaran O. A., Nature Physics **4** (2), 149–154 (2007).

11. Cloupeau M. and Prunet-Foch B., Journal of Electrostatics **22** (2), 135–159 (1989).

12. Fenn J. B., Mann M., Meng C. K., Wong S. F. and Whitehouse C. M., Science **246** (4926), 64–71 (1989).

13. Brazier-Smith P. R. and Jennings S. L. J., Q J R Meteorol Soc **99** (422), 776–786 (1973).

14. Lee D.-Y., Shin Y.-S., Park S.-E., Yu T.-U. and Hwang J., Applied Physics Letters **90** (8), 081905 (2007).

15. Taylor G. I., Proceedings of the Royal Society of London. Series A. Mathematical and Physical Sciences **291** (1425), 159–166 (1966).

16. Melcher J. R. and Taylor G. I., Annual Review of Fluid Mechanics **1** (1), 111–146 (1969).

17. Saville D. A., Annual Review of Fluid Mechanics **29** (1), 27–64 (1997).

18. Zholkovskij E. K., Masliyah J. H. and Czarnecki J., Journal of Fluid Mechanics **472**, 1–27 (2002).

19. Schnitzer O. and Yariv E., Journal of Fluid Mechanics **773**, 1–33 (2015).

20. Bazant M. Z., Journal of Fluid Mechanics **782**, 1–4 (2015).

21. Mori Y. and Young Y.-N., Journal of Fluid Mechanics **855**, 67–130 (2018).

22. Geng H., Feng J., Stabryla L. M. and Cho S. K., Lab on a Chip **17** (6), 1060–1068 (2017).

23. Jia Y., Ren Y., Hou L., Liu W., Deng X. and Jiang H., Small **13** (46), 1702188 (2017).

24. Loscertales I. G., Barrero A., Guerrero I., Cortijo R., Marquez M. and Gañán-Calvo A. M., Science **295** (5560), 1695–1698 (2002).

25. Song R., Abbasi M. S. and Lee J., Microfluidics and Nanofluidics **23** (7), 92 (2019).

26. Tucker-Schwartz A. K., Bei Z., Garrell R. L. and Jones T. B., Langmuir **26** (24), 18606–18611 (2010).

27. Xie J., Jiang J., Davoodi P., Srinivasan M. and Wang C.-H., Chemical Engineering Science **125**, 32–57 (2015).

28. Bhaumik S. K., Roy R., Chakraborty S. and DasGupta S., Sensors and Actuators B: Chemical **193**, 288–293 (2014).

29. Wehking J. D. and Kumar R., Lab on a Chip **15** (3), 793–801 (2015).

30. Xi H.-D., Guo W., Leniart M., Chong Z. Z. and Tan S. H., Lab on a Chip **16** (16), 2982–2986 (2016).

31. Guan X., Hou L., Ren Y., Deng X., Lang Q., Jia Y., Hu Q., Tao Y., Liu J. and Jiang H., Biomicrofluidics **10** (3), 034111 (2016).

32. Huo M. and Guo Y., Polymers **12** (2), 335 (2020).

33. Lecuyer S., Ristenpart W. D., Vincent O. and Stone H. A., Applied Physics Letters **92** (10), 104105 (2008).

34. Nguyen V. D. and Byun D., Applied Physics Letters **94** (17), 173509 (2009).

35. Panov V. A., Kulikov Yu. M., Vetchinin S. P., Pecherkin V. Ya. and Vasilyak L. M., Plasma Sources Sci. Technol. **32**, 095020 (2023).

36. Panov V. A., Vasilyak L. M., Pecherkin V. Ya., Vetchinin S. P. and Kulikov Yu. M., Applied Physics, No. 4, 5–10 (2022) [in Russian].

37. Panov V. A., Kulikov Yu. M., Pecherkin V. Ya., Vasilyak L. M. and Saveliev A. S., Applied Physics, No. 6, 5–10 (2023) [in Russian].

About authors

Vladislav Aleksandrovich Panov, Senior Research Assistant, Candidate of Physics and Mathematics, Joint Institute for High Temperatures of the Russian Academy of Sciences (125412, Russia, Moscow, Izhorskaya Ulitsa, 13, bld. 2). E-mail: panovvladislav@gmail.com SPIN code 5821-2776, Author ID 755538

Andrei Sergeevich Saveliev, Senior Research Assistant, Candidate of Physics and Mathematics, Joint Institute for High Temperatures of the Russian Academy of Sciences (125412, Russia, Moscow, Izhorskaya Ulitsa, 13, bld. 2). E-mail: fisteh@mail.ru SPIN code 6888-7369, Author ID 866343

Yurii Matveevich Kulikov, Senior Research Assistant, Candidate of Physics and Mathematics, Joint Institute for High Temperatures of the Russian Academy of Sciences (125412, Russia, Moscow, Izhorskaya Ulitsa, 13, bld. 2). E-mail: kulikov-yurii@yandex.ru SPIN code 7719-8459, Author ID 1130937